Available online at www.sciencedirect.com
ScienceDirect
International Journal of Mass Spectrometry 258 (2006) 120–133
International Journal of Mass Spectrometry
www.elsevier.com/locate/ijms

A comprehensive characterization of photoelectron resonance capture ionization aerosol mass spectrometry for the quantitative and qualitative analysis of organic particulate matter

Brian W. LaFranchi, Giuseppe A. Petrucci *

A-218 Cook Physical Sciences, Department of Chemistry, University of Vermont, Burlington, VT 05405, USA

Received 11 May 2006; accepted 7 June 2006
Available online 1 August 2006

Abstract

Photoelectron resonance capture ionization (PERCI), when coupled with thermal vaporization aerosol mass spectrometry (AMS) is found to be an excellent ionization method for the identification of particle-bound organics. While the qualitative analytical advantages of PERCI have been demonstrated previously, a comprehensive characterization of PERCI-AMS, which will be of paramount importance in developing the method to perform reliable quantitative measurements, is discussed here. A detailed analysis, based on photoelectron, gas phase, and particle phase measurements, of the behavior and limitations of PERCI-AMS is given. The performance of PERCI-AMS is affected by: delayed time between anion formation and extraction for mass spectral analysis, relative positioning of the vaporization probe (VP) and photoelectrode (PE), laser intensity, analyte pressure in the ionization region, particle matrix, and vaporization temperature ramping rate. Gas phase detection limits are found to be on the order of 10^7–10^9 cm^{-3} and particle phase detection limits for individual compounds are found to be on the order of 10^{-8}–10^{-7} g of total sampled mass. An additional level of analyte selectivity is gained with the vapor pressure dependent desorption of deposited particles, achieved with ramped thermal vaporization. The major limitation of the thermal vaporization PERCI-AMS is the low duty cycle of the measurement, stemming from the pulsed nature of PERCI. Finally, prospects for improvements in detection limits as high as 3–4 orders of magnitude by adaptation of pulsed IR laser desorption to the system are discussed.

Keywords: Aerosol mass spectrometry; Photoelectron resonance capture ionization; Organic aerosol; Soft ionization; Photoelectron emission

1. Introduction

Important advances in our understanding of the Earth's atmosphere have been made with the advent of on-line and real-time measurements of airborne particulates. Specifically, on-line aerosol mass spectrometry (AMS) has found significant success in addressing important atmospheric issues [1,2]. A commonly cited limitation of aerosol mass spectrometry has been its inability to adequately analyze the organic fraction of atmospheric particulates [1]. Generally making up around 20–50% of the total fine aerosol mass, organic aerosol is thought to play an important role in climate forcing [3–13], atmospheric chemistry [14–17], and human health [18–24]. According to a recent report [25] however, only about 10% of the organic compounds in organic atmospheric aerosols have been identified. Until recently, aerosol mass spectrometers have relied on multi-photon laser ionization or electron impact ionization [26–31]; however, molecular fragmentation caused by these ionization methods can limit their utility to provide organic compound identification. A few novel approaches have been used to improve the capabilities of these "conventional" ionization sources through deconvolution of complex mass spectral data [32,33], vapor pressure dependent desorption of deposited particles [34], and tandem mass spectrometry [35].

Alternate ionization schemes in AMS are being developed with the express purpose of addressing the limitation of molecular identification of particle-bound organics. These so-called soft-ionization methods are characterized by minimal molecular fragmentation, thereby allowing for more facile identification of individual organic molecular components. Two such methods include chemical ionization [36–39] and vacuum ultraviolet (VUV) single photon ionization (SPI) coupled with IR laser

* Corresponding author. Tel.: +1 802 656 0957; fax: +1 802 656 8705.
E-mail address: Giuseppe.Petrucci@uvm.edu (G.A. Petrucci).

1387-3806/$ – see front matter © 2006 Elsevier B.V. All rights reserved.
doi:10.1016/j.ijms.2006.06.013

vaporization [40,41]. This paper describes an alternative soft-ionization scheme, photoelectron resonance capture ionization (PERCI) that has been under development and in use in our laboratory for several years and provides unique capabilities in aerosol analysis.

PERCI-AMS has been applied successfully to the direct analysis of particle-bound organics, as a result of the minimal fragmentation that occurs during the ionization process. PERCI relies on the capture of low energy photoelectrons generated by the action of a pulsed UV laser on a metal surface under vacuum. The nominal energy of the photoelectrons (ε_{pe}) is governed by the difference in energy between the incident photons ($h\nu$) and the metal work function (ϕ) as follows: $\varepsilon_{pe} = h\nu - \phi$.

At low values of ε_{pe} (<10 eV), a wide variety of classes of molecules can undergo electron attachment through either an associative or dissociative mechanism [42], forming the negative molecular ion or fragment ion, respectively. Known as resonance electron capture (REC), this type of ionization has been discussed in the literature (for an excellent review see Chutjian et al. [42]). It has proven to be a useful ionization method for organic molecules functionalized with halogens [43–45], nitrates [46–48], sulfur [49,50], conjugated π-systems [51] and carbonyls [52], as well as straight-chain hydrocarbons with minimal functionality [53]. Two common methods of generating low energy electrons controllably are with a trochoidal electron monochromator [54] or with a reversal electron attachment detector (READ) [44], both of which generate continuous electron beams of 0.5–2 μA and 400 μA, respectively. The advantage of using PERCI over these methods lies with the high instantaneous photoelectron currents ($\sim 10^2$ mA in 5 ns) produced by the pulsed laser, making PERCI a nearly ideal ionization source for time-of-flight mass spectrometry.

We have published on the utility of PERCI as a soft-ionization technique for gas-phase organics [55] and as a suitable method, when coupled with thermal vaporization, for monitoring ozonolysis products of oleic acid particles [56]. Additionally, we have used PERCI-AMS to study the reaction mechanisms leading to high molecular weight oxygenates [57] and polymerization [58] in the heterogeneous oleic acid/ozone system and to identify a complex series of reaction products resulting from the heterogeneous ozonolysis of mixed fatty acid/methyl ester particles [59]. We have also applied PERCI to the analysis of olive oil [60] and biodiesel (discussed here in Section 3.4), as well as model and real ambient aerosols (unpublished work). In all of these cases, PERCI has been found to be a powerful technique in identifying molecular components in the particle phase, especially for the analysis of complex chemical mixtures.

While most of these reports have focused on qualitative and semi-quantitative applications of PERCI-AMS, ultimately it will be of primary importance to optimize the system for quantitative measurements. Towards this end, it is important to understand the fundamentals of the PERCI process; specifically, it is necessary to understand how the PERCI source is coupled to the particle vaporization source as well as the time-of-flight ion optics. Some of the questions that must be answered include: what factors affect the measured ion signal intensity; what is the effect of the vaporization source in the ion extraction region on ion detection; what is the ideal placement of the photoelectrode (PE) and vaporization source in the ion extraction region; and what is the best way to vaporize the particles. A combination of photoelectron current, gas phase, and particle phase measurements designed to answer these questions are described in this work.

We report here on the current state of the PERCI-AMS instrumentation and methodology as applied to the analysis of organic aerosols, including the fundamentals of the PERCI process and some key analytical figures of merit. The limitations and potential for future design and optimization of the PERCI-AMS are also discussed.

2. Experimental

2.1. General instrument description

Typical operational details of the PERCI-AMS have been described previously [55–58]; however, additional details are given here that are pertinent to the ensuing discussion which describes photoelectron and gas phase measurements as well as particle phase studies. A schematic of the PERCI-AMS is shown in Fig. 1(a).

The ionization source consists of a low energy (sub-mJ) pulsed (10 Hz), tunable (235–300 nm) ultraviolet laser (Opotek Inc., Carlsbad, CA) focused to ∼1 mm (providing a fluence of $\sim 10^2$ mJ/cm^2) onto the surface of a pure aluminum photoelectrode, generating a short (5 ns) burst of photoelectrons. A vaporization probe (VP) (see Section 2.4) is placed in close proximity to the PE and intercepts the particle beam for aerosol measurements. Vaporization and analysis is done after collecting sampled aerosol on the VP (at room temperature) for a short time. Mass analysis of the PERCI anions is performed with a time-of-flight mass spectrometer (R. M. Jordan, Inc., Grass Valley, CA) operating in reflectron mode. The ion extraction zone consists of a symmetric Wiley-McLaren arrangement with delayed pulse ion extraction (DPE), where the extraction electrodes are held at ground potential while the ionization laser is fired and then pulsed using a digital pulse generator (model DG535; Stanford Research Systems, Inc., Sunnyvale, CA) coupled with a high voltage pulsed power supply (+/−950; model PVM-4210; Directed Energy, Inc., Fort Collins, CO). Delay times used in these experiments range from hundreds of nanoseconds up to 10 μs. Data is acquired in time at 1 GS/s using a digital oscilloscope (WavePro 7000, LeCroy, Chestnut Ridge, NY). The pulse generator also controls the timing of the data acquisition, triggering the scope at the same instant that the extraction electrodes are pulsed. The oscilloscope can be further triggered to save individual mass spectra when ions are present in a given mass range or at an individual m/z.

Fig. 1(b) is a diagram showing a close-up of the ionization region along with the positions of the PE and VP. Both the PE and VP are on precision translational mounts; the PE can be moved linearly along the diagonal of the extraction electrode, while the VP can be moved in the x, y, and z directions. The y- and z-axes are shown in the diagram and will be referred to in this discussion. The x direction is normal to the plane of the ion

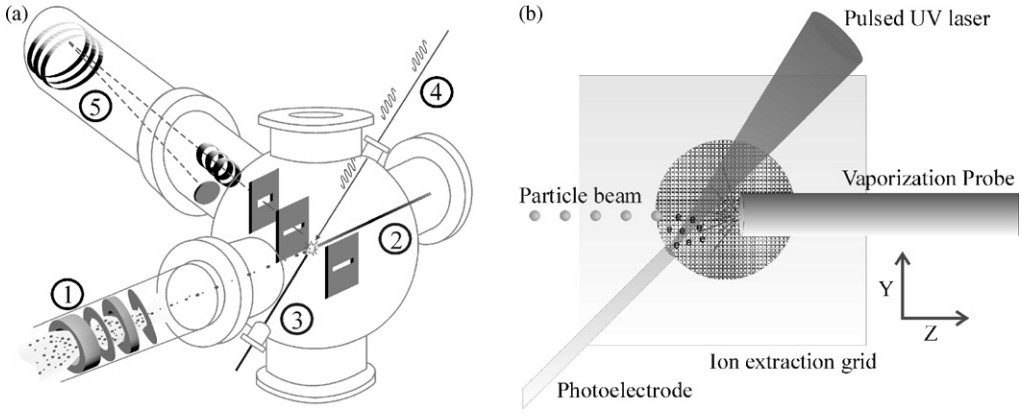

Fig. 1. (a) Schematic of PERCI-AMS, which consists of five main components: (1) particle inlet; (2) particle collector/vaporization probe (VP); (3) aluminum photoelectrode (PE); (4) tunable UV pulsed laser; and (5) time-of-flight mass spectrometer along with necessary electronics and data processing equipment. (b) Close-up of ion extraction region consisting of photoelectrode, vaporization probe, and ion extraction electrode.

extraction electrode and the components are generally not moved in this direction during these experiments once everything is aligned. The PE is 1 mm in diameter; the VP is mounted to the end of a ~3 mm diameter double-bore ceramic tube containing copper leads for the nichrome coil; the ion extraction electrodes are 4 cm × 4 cm and the circular grid through which ions are extracted is 1 cm in diameter. The PE and VP are held roughly in the center of the two extraction grids (only one shown in Fig. 1(b)) along the *x*-axis, which are separated by 2 cm. The laser beam is directed normal to the PE surface and focused using a 30 cm quartz lens. The gradual focus produces a fairly homogeneous beam profile through the ionization region. This is important to ensure that the laser intensity does not change significantly as the PE position is changed.

2.2. Photoelectron measurements

Measurements of photoelectron fluxes were made in two different ways: (a) indirectly, as electron current flows from ground across a 1.5 Ω resistor to replenish the photoelectrons ejected from the surface of the PE and (b) directly, by holding a conducting probe at known distances from the surface of the PE, held under vacuum. In general, the first method was useful in providing some idea of the number of photoelectrons generated while the second approach gave information on the spatial distribution of the photoelectrons at various distances away from the photoelectrode.

The nichrome wire on the VP (see Section 2.4) was a suitable probe for direct detection of the photoelectrons. The photoelectron current, for both approaches, was measured using the oscilloscope while acquiring at 5 GS/s. The temporal evolution of the photoelectron pulses in both experiments was found to follow the laser pulse closely (FWHM ~5 ns). The photoelectron count was determined by taking the integrated area of the photoelectron current peak, which is in units of nanovolt-seconds, dividing by the resistance of the circuit and then by the charge of an electron (1.602×10^{-19} *C*). As will be discussed in Section 3.1.1, the photoelectron current in both cases was found to be dependent upon the potentials applied to the TOF-MS ion optics, especially the extraction plates and the adjacent acceleration plates. Because ions were not being detected during these experiments, the potential on these plates could be adjusted as needed using the DC power supplies for the TOF-MS.

2.3. Gas phase sampling and measurement

Gas phase analyte was introduced into the ionization chamber using a precision leak valve (model ULV-150; MDC Vacuum Products Corp., Hayward, CA), not depicted in Fig. 1. Three reference compounds with high vapor pressure were used in this study: 2-nitrophenol (98% from Avocado Research Chemicals, Inc., Lancashire, UK), 2-ethyl hexyl nitrate (97% from Sigma–Aldrich, Milwaukee, WI), and 1-nitronaphthalene (99% from Sigma–Aldrich, Milwaukee, WI). All chemicals used for gas phase analysis in these experiments were sufficiently volatile to vaporize under moderate vacuum with no heating necessary. Grinding the 2-nitrophenol into a fine powder facilitated vaporization. The pressure of analyte in the ionization chamber was monitored continuously using a Combivac CM 31 pressure gauge (Leyblod, Koln, Germany) and maintained between 10^{-7} and 10^{-5} Torr. Unless otherwise noted, all results presented for gas phase measurements reflect the average TOF-MS signal from 100 laser shots.

2.4. Aerosol sampling

Polydisperse aerosols were produced by pneumatic nebulization of dilute solutions of analyte in ethanol or a 15% (v/v) ethanol/water mixture. Oleic acid (99%) was obtained from Mallinckrodt-Baker, Inc., (Paris, KY), and all other chemicals (triolein (99%), glutaric acid (99%), azelaic acid (98%), and dioctyl sebacate (DOS) (97%)) were obtained from Sigma–Aldrich (Milwaukee, WI). A biodiesel sample was obtained from Green Technologies, LLC (Winooski, VT). All chemicals were used without further purification. Number and mass size distributions of the resulting aerosol were recorded in parallel with all quantitative measurements using a scanning mobility particle sizer (SMPS) (Model 3080, TSI, Inc., Shoreview, MN), consisting of a differential mobility analyzer (DMA) to size the particles and a condensation particle counter

(CPC) to count them. Particle flow upstream of the PERCI-AMS inlet was maintained, whether sampling or not, using an overflow outflow through a HEPA filter. With this arrangement, the SMPS could make measurements continuously, independent of whether the PERCI-AMS is sampling. Aerosol mass concentrations, as determined by the SMPS, were monitored over the course of a particular experiment for stability and also to determine the total amount of material sampled during any given aerosol deposition experiment. Monodisperse aerosols were sampled into the PERCI-AMS from the outlet of the DMA. Simultaneous monitoring of monodisperse particle concentrations was performed with the CPC while sampling into the PERCI-AMS.

Aerosol particles were introduced into the mass spectrometer through a differentially pumped inlet and focused into a beam using a series of three aerodynamic lenses [61–63]. A 220 μm diameter critical orifice at the entrance of the aerodynamic lens maintained an aerosol sampling flow rate of 0.45 L/min. For the quantitative experiments described here, the operating conditions for the inlet were maintained in an optimized configuration for transmitting a wide range of particle sizes.

2.5. Particle vaporization and measurement

Two different vaporization source designs were used, the main operational difference being the maximum temperature ramping rate possible. Both designs consisted of a nichrome filament (AGW 30) wrapped into a 4-turn coil. In one design, the coil was wrapped around a heat-conducting ceramic cylinder (radius ∼2 mm, length ∼4 mm) constructed from Resbond 919 electrically resistant ceramic adhesive (Cotronics Corp., Brooklyn, NY). A type-k thermocouple junction was embedded into the heat-conducting ceramic. In the second design, the thermocouple was potted on the inside of the nichrome coil with a small amount of Resbond 919. This latter design was found to be more efficient since there was less ceramic mass that required heating, allowing ramping rates up to 25 °C/s; whereas the former was limited to 10 °C/s. With both designs, a CN8201 series Omega (Stamford, CT) temperature controller was used to monitor the temperature of the ceramic and to regulate the DC current applied to the filament. The maximum temperature used in all experiments was 400 °C, well above the atmospheric pressure boiling points of the compounds studied. This temperature was found to be just below the point where the nichrome wire starts to glow red and a substantial amount of electronic noise occurs at the MCP detector. There was some delay in transferring the heat from the filament to the ceramic, apparent with both designs. Therefore, the temperature measured by the thermocouple embedded in the ceramic lagged behind the temperature of the filament, especially during a quick temperature ramp. The result was a quick burst in signal at the very beginning stages of the temperature ramp, presumably, as the deposited aerosol components that are in direct contact with the filament were vaporized first. The remaining deposited aerosol then vaporized as the temperature of the ceramic cylinder increases. The vaporization source could also be operated in "flash-vaporization" mode at a fixed temperature where the impacting particles were instantaneously vaporized.

Quantification of deposited particulate compounds was performed by determining the instrumental response (R), which was calculated from the TOF-MS ion signal height from successive laser pulses integrated over time during the vaporization temperature ramp. The background noise (σ_{bg}) was calculated by taking repetitive measurements of R with no aerosol deposited, integrating the signal for a given m/z over the appropriate time range, and calculating the standard deviation of these measurements. Detection limits ($3\sigma_{bg}$) were calculated by obtaining R from a known amount of sampled particulate mass, as determined from the inlet flow rate, the sampling time, and the aerosol mass distribution. In the results presented here, the detection limits are expressed as a total amount of mass sampled, which can be extended to an atmospheric mass concentration for any given sampling time.

The error bars for R on all of the particle phase measurements in this report were determined from the average relative standard deviation (R.S.D.) for pure oleic acid over 10 successive measurements. The R.S.D. for these measurements generally ranged from 15 to 25% of the total response.

3. Results and discussion

3.1. Photoelectron emission

PERCI relies on the resonant capture of low energy electrons by molecules. Photoelectron flux densities impact the analytical performance and sensitivity of PERCI. Ideally, a high quantum efficiency is sought to maximize conversion of photons to photoelectrons, thereby increasing flux densities and enhancing the ionization rate. Additionally, the spatial distribution of photoelectrons with respect to the other elements in the TOF-MS extraction region will govern the overlap of photoelectrons with analyte vapors, affecting the ionization efficiency. This section will focus on the characterization of the photoelectrons generated in the PERCI source with respect to their flux density and spatial distribution.

3.1.1. Photoelectron emission flux density

The quantum efficiency for photoelectron emission, η_{pe}, is a function of extraction field strength and photon wavelength (Fig. 2). Nominally, one would expect η_{pe} to be dependent only on the PE material surface; however, there are two experimental factors that impact the observed dependence: (1) the instantaneous mirror potential developed at the PE surface upon photoelectron emission; and (2) the space charge developed above the surface as a function of the large photoelectron flux densities generated by the UV laser pulse. Both of these factors present a barrier to ejection of photoelectrons. Therefore, as shown in Fig. 2, one would predict that photoelectrons with higher kinetic energies, i.e., shorter UV wavelengths, would escape the surface with greater probability. At each laser wavelength, one extraction electrode was held at 0 V while the other was increased gradually up to 3000 V, giving a field strength within the two electrodes ranging from 0 to +1500 V cm^{-1}. At a field strength

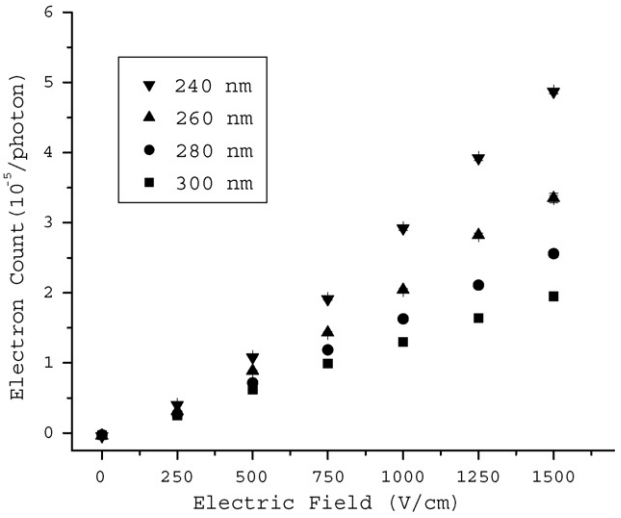

Fig. 2. Photoelectron count at 240, 260, 280, and 300 nm plotted as a function of applied electric field. Error bars for these measurements are smaller than the dimensions of the symbols.

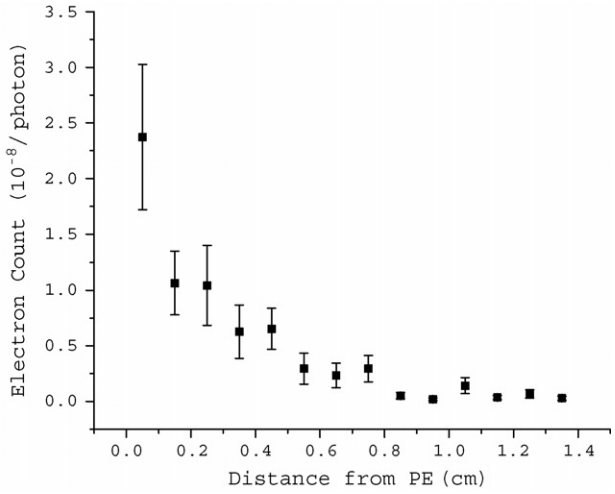

Fig. 3. Photoelectron current collected at different distances from the photoelectrode (PE). Laser wavelength = 270 nm.

of 1500 V cm^{-1}, the η_{pe} for the wavelengths studied here ranged from 2 to 5 × 10^{-5} photoelectrons/photon.

The quantum efficiency for the aluminum PE used in this study was measured experimentally to be 4.9 × 10^{-5} at the highest applied field of 1500 V cm^{-1} and a wavelength of 240 nm. This is in good agreement with reported values of 9 × 10^{-5} [64]. The discrepancy between the two values is likely due to the much higher photoelectron extraction electric field of 5 kV cm^{-1} used by Kawamura et al. [64], which would increase the number of electrons extracted and counted. In this work, the lower extraction field resulted in some of the photoelectrons being redeposited onto the PE, as described above.

The quantum efficiency measured under the influence of an electric field represents an upper limit to the effective photoelectron flux (i.e., photoelectrons that are available for capture by analyte); defining the effective photoelectron flux density is not straightforward because it will depend on the strength of the extraction field (if any) and the distance from the PE surface (as a result of the spatial dimensions of the electron cloud) where ionization takes place. Under conditions of mass spectrometric analysis, where delayed pulse extraction is used, there exists no photoelectron extraction field during the laser pulse. Further, in the absence of analyte molecules, no photocurrent is measured (i.e., essentially all emitted photoelectrons are returned to the PE surface.) In the presence of analyte, some of the emitted photoelectrons are captured, resulting in the formation of measurable molecular anions; however, this small fraction of captured photoelectrons does not result in a directly measurable photocurrent with our experimental set-up. As a result, it has not been possible to measure, directly, the effective quantum efficiency (i.e., useful photoelectrons per photon) under actual PERCI-AMS measurement conditions.

3.1.2. Photoelectron spatial distribution

In the absence of an electric field to extract emitted photoelectrons, a strong space charge develops above the PE surface as a result of the large electron densities and the majority of photoelectrons are returned to that surface. The distance that the electrons travel before inverting their direction, called the "turn around distance" (typically a few micrometers [65]) is dependent upon the initial electron density at the PE surface and the average electron energy. A relevant result of this effect is that under field-free conditions, the highest electron density exists in a small volume (∼10^{-4} mm^3) immediately above the PE surface (defined by the area of the PE surface and the turn-around distance of the photoelectrons), leading to the hypothesis that molecular ionization occurs in this volume (see below for detailed discussion).

In order to characterize the region of molecular ionization in the volume above the PE surface, the emitted photoelectron current in space was detected using a conducting probe placed at known distances from the PE surface. First, the PE position was fixed and the VP was scanned in the z direction as shown in Fig. 1(b). The photoelectron current increases as the probe is brought closer to the PE, as expected (Fig. 3). Approximately 3 orders of magnitude fewer photoelectrons are measured per laser pulse as compared to the number of photoelectrons that initially escape the PE surface. Two possible reasons for the reduced electron count as one moves away from the PE surface are that (1) the electrons are formed essentially at a point and disperse in space as they travel outward, radially. This can likely account for a loss in photoelectron current of about 1 order of magnitude at the most (ratio of areas of emitting and collecting surfaces); and (2) the majority of the photoelectrons may be redirected to the PE surface. These observations support the hypothesis that there is a significantly greater probability for ionization to occur closer to the PE surface.

3.2. Anion energetics

The relative intensity of a given anion is dependent upon the delayed pulse extraction time (τ_d), that is the time lag between the ionizing laser pulse and the ion extraction pulse

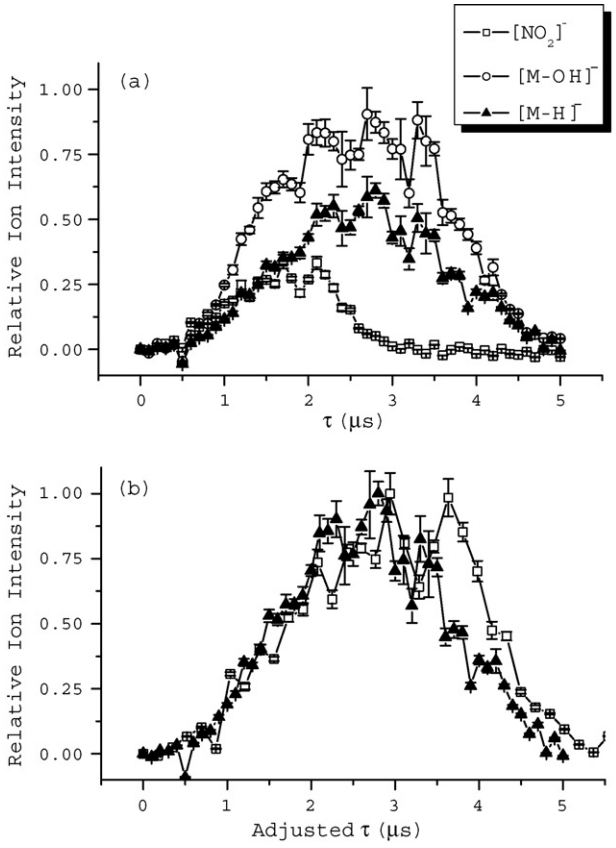

Fig. 4. (a) Behavior of three ion fragments of 2-nitrophenol with delayed pulse extraction time (τ). (b) Data in (a) plotted with the $[NO_2]^-$ ion adjusted to compensate for the difference in mass between it and the $[M-OH]^-$ ion. Ion intensities are normalized to 1 for both ions. Overlap of adjusted plots shows that kinetic energy for both ions are identical and differences in optimal DPE times are a result of differences in velocity. Laser wavelength = 280 nm; pressure = 2×10^{-5} mbar.

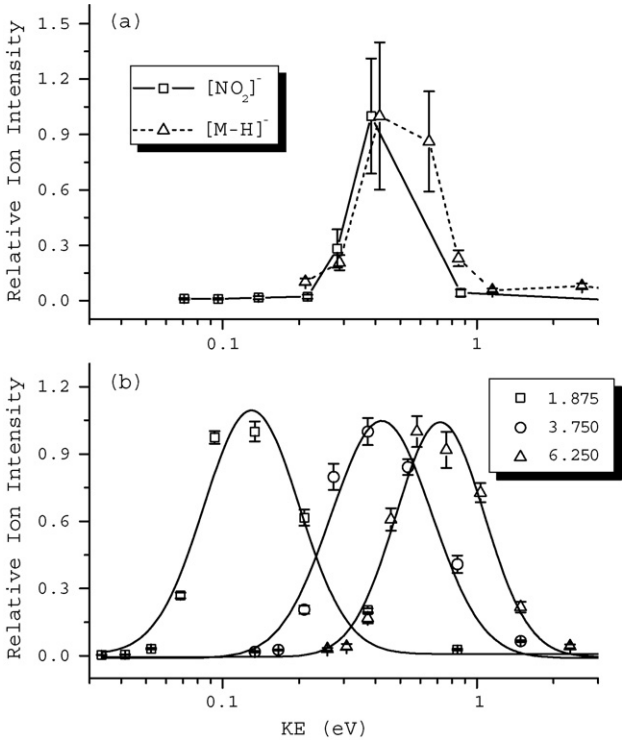

Fig. 5. (a) Kinetic energy plots for two fragment ions ($[NO_2]^-$ and $[M-OH]^-$) from 2-nitrophenol obtained simultaneously. Ion intensities are normalized to 1. (b) Kinetic energy profiles along with log-normal fits for $[NO_2]^-$ ion at variable photoelectrode (PE) positions. Distances are given in millimeters measured from the center of the extraction region. Pressure = 9×10^{-7} mbar; laser wavelength = 270 nm.

(e.g., Fig. 4(a) for the case of 2-nitrophenol). For optimal ion signal intensities higher mass ions require greater delay times than lower mass ions. The decrease in all ion signals at relatively high τ_d reflects ion diffusion out of the collection region. Assuming equal ion kinetic energies upon formation, higher mass ions (which will have lower velocity) will remain in the ion extraction volume for a longer period of time than the lighter ions, resulting in a broader DPE curve. For example, the half-widths of the DPE curves for $[NO_2]^-$ and $[M-H]^-$ at 280 nm are 1.2 and 2.5 μs, respectively. Identical behavior was reproduced at wavelengths of 290 and 260 nm. In these experiments, the anticipated lifetimes of the measured anions are on the order of τ_d and the ion flight time (i.e., 10–100 μs) [66–68]. Therefore, no significant losses in ion signal are expected over this measurement range due to anion lifetimes.

The DPE curves likely mirror the diffusion of ions, formed within a few micrometers of the PE surface, into and out of the optimal ion extraction zone of the mass spectrometer. Ion kinetic energies can be calculated by measuring the optimal τ_d for the different ions [69]. The τ_d yielding the maximum ion signal is a function of the ion kinetic energy ($1/2mv^2$) and the position of the PE surface relative to the ion extraction zone. The travel time for one ion to reach a given position (t_1) is related to the time (t_2) it takes for a second ion to reach that same position through the equation: $t_1 = t_2(m_1/m_2)^{1/2}$, where m_1 and m_2 are the masses of the two ions. Taking the $[M-H]^-$ (138 m/z) and $[NO_2]^-$ (46 m/z) ions from 2-nitrophenol as an example, there should be a separation in time of the two DPE curves by a factor of $3^{1/2}$ or 1.73. If this factor is applied to the $[NO_2]^-$ τ_d values, a good agreement is obtained between the two DPE curves (Fig. 4(b)), supporting our hypothesis that, regardless of mass, ions are formed at the PE surface with identical energies.

For ion generation at a given point in space, therefore, the nominal initial kinetic energies are essentially equal for all ions. For example, the average kinetic energy of both the $[NO_2]^-$ and $[M-H]^-$ ions, measured at a distance of 3.8 mm from the center of the ion collection region (Fig. 5(a)) is estimated to be about 0.5 eV. However, this KE is also dependent on post-acceleration due to stray electric fields. For example, Fig. 5(b) shows the calculated ion kinetic energies for the $[NO_2]^-$ anion as a function of PE position relative to the ion collection region. There is a clear increase in ion kinetic energy, from 0.1 eV at 1.88 mm to 0.7 eV at 6.25 mm, indicating acceleration of the ions after formation. Although accurate knowledge of stray electric fields within the ion source is not essential for fields of low magnitude, their presence must be accounted for by determination of the optimum τ_d.

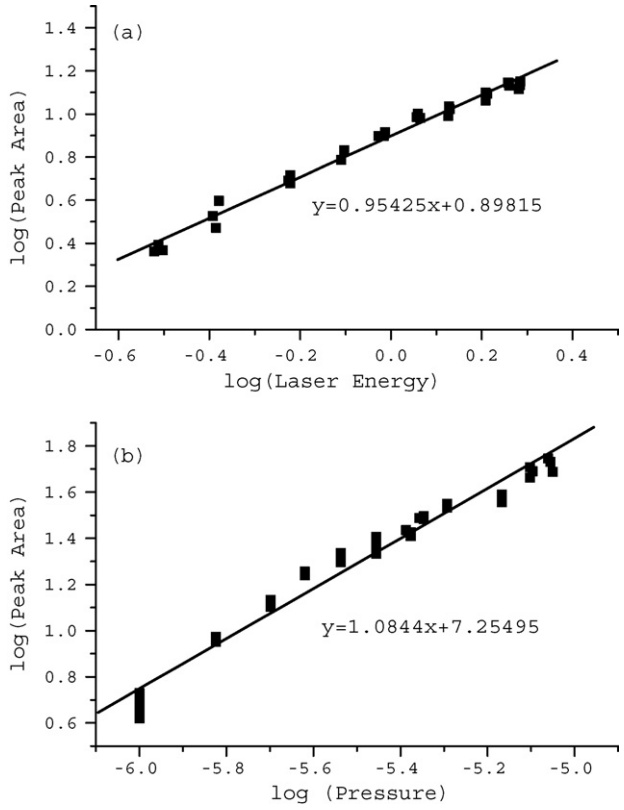

Fig. 6. Log–log plots of ion signal peak area for $[M-OH]^-$ ion from 2-nitrophenol vs. (a) laser pulse energy and (b) analyte pressure (in mbar). Slope of best fit line shows first order relationships in both cases. Laser wavelength = 270 nm.

3.3. PERCI analytical performance

3.3.1. Gas phase limits of detection

The analytical figures of merit of PERCI were evaluated first for gas phase samples. The anion signal for 2-nitrophenol was linearly dependent on laser intensity (i.e., photoelectron flux) (Fig. 6(a)) indicating a single photon absorption photoelectron emission. Signal saturation was not observed as a function of laser intensity, the maximum being limited by breakdown at the PE surface. The signal was also linearly dependent on analyte vapor pressure between about 10^{-6} and 10^{-5} mbar (Fig. 6(b)). Pressure measurements below 10^{-6} mbar are unreliable with our system, and linearity suffers, as a result, while the operational constraints of the TOF-MS and associated electronics limited an extension of this experiment to higher pressures. Extrapolating the data in Fig. 6(b) provides a limit of detection ($3\sigma_{bg}$, 100 averages) for 2-nitrophenol ($[M\text{-}17]^-$) of 1.6×10^7 cm^{-3}. Analogous experiments on other compounds provided limits of detection of 2.9×10^9 and 3.5×10^7 cm^{-3} for ethyl hexyl nitrate ($[M\text{-}48]^-$) and 1-nitronaphthalene ($[M]^-$), respectively (ion measured is shown in parentheses). The lower detection limit for 1-nitronaphthalene is likely explained by its additional aromaticity, which has been found previously to be associated with improved electron capture cross sections [70]. This highlights the prospects for using PERCI as a sensitive ionization method for polycyclic aromatic hydrocarbons of environmental relevance. Note that for these experiments, the VP was in place, but not used.

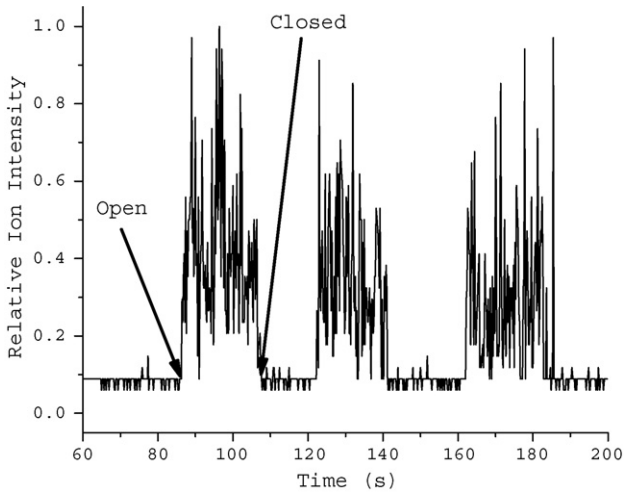

Fig. 7. Flash-vaporization of oleic acid particles as a valve upstream of the particle inlet is alternated between particle free air (closed) and oleic acid aerosol (open). Signal trace is monitored at 281 *m/z* or $[M-H]^-$ ion. Particle mass concentration was 1.8×10^4 μg/m^3. Laser wavelength = 270 nm.

3.3.2. Vaporization probe alignment

Oleic acid (9-octadecenoic acid) is an ideal test compound for evaluating the analytical capabilities of the PERCI-AMS for aerosol analysis, since it is know to form spherical particles that are transmitted efficiently through the particle inlet, it is sensitive to electron capture [56], and it is atmospherically relevant [71]. Fig. 7 shows a trace of the $[M-H]^-$ (281 *m/z*) ion signal as pure oleic acid particles are introduced into the PERCI-AMS. During this measurement, particles are flash-vaporized as they impact the vaporization source held at 200 °C. The 281 *m/z* signal rises and rapidly drops to baseline with opening and closing the valve controlling aerosol flow to the inlet, with no evidence of any significant memory effect when particles are sampled and measured in this fashion. The unusually large shot-to-shot fluctuations observed, while particles are being sampled, are likely a result of the variability in the mass of molecular vapor in the ionization region during the ionization pulse. This stems mainly from the variability in temporal overlap between impacting particles and the ionization pulse (see Section 3.4 for a more detailed discussion). An average mass concentration sampled into the PERCI-AMS can be determined; however, normal fluctuations on the time scale of the PERCI-AMS measurements cannot be independently monitored.

Alignment of the vaporization probe is critical to maximize the instrumental response for particle phase measurements. In addition to the need for alignment of the incoming particle beam with the vaporization probe, it was also found that there is an optimum separation between the photoelectrode and vaporization probe. From gas phase experiments, where confounding factors associated with particle sampling, collection, and vaporization are eliminated, it was determined that regardless of the relative positions of the PE and VP in the extraction region, ion signals are enhanced when the PE and VP are separated by

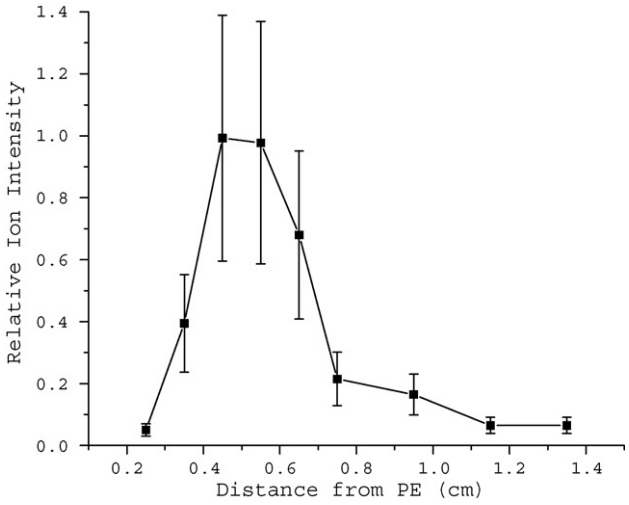

Fig. 8. Oleic acid ion intensity resulting from flash-vaporization as a function of the vaporization source distance from the photoelectrode (PE). Particle mass concentration was 1.8×10^4 μg/m^3. Laser wavelength = 270 nm.

a distance of about 5 mm. Further, anion signals disappear to background levels at a separation of less than a few millimeters. Therefore, the optimum distance for particle sampling must be compromised to maximize overlap of the expanding vapor cloud with the PE surface while maintaining enough separation to minimize the interferences observed with gas phase measurements.

To address the issue of VP alignment, flash vaporization of oleic acid particles was performed while monitoring the $[M-H]^-$ intensity as a function of VP position, relative to the PE (cf. Fig. 8). The $[M-H]^-$ intensity starts to increase at a separation distance of 7 mm, where the molecular vapors start to significantly overlap with the electrons located at the PE surface. The anion intensity reaches a maximum at 5 mm and then decreases as the VP is brought closer to the PE. At distances closer than 5 mm, the interference described previously for gas phase measurements starts to negate any additional improvement in molecule/electron overlap. Presumably, in the absence of this interference, the intensity from particle phase analytes would continue to increase as this distance is decreased, since the overlap between the vapor plume and the photoelectrons is improved. It will be critical, therefore, in future work, to determine the source of this interfering effect, as improved detection limits for particle phase species may result from better overlap of the vaporized molecules with the PE surface.

3.3.3. Vaporization probe temperature programming

While flash vaporization provides real-time analysis of aerosols, it can be beneficial to deposit sampled particles onto the VP, held at room temperature or lower, over some reasonable length of time in order to improve detection limits. In theory, particles can be collected for whatever amount of time is feasible for a particular application; however, the deposit time will ultimately be limited by evaporation rate of the deposited particles. No significant evaporation has been found to occur in our system with oleic acid particles using deposit times as high as 5 min. Subsequent temperature ramping allows for a controlled sampling of the entire deposited particle mass at one time. Fig. 9(a and b) show the real-time 281 *m/z* anion intensity from collected oleic acid particles over the course of the temperature ramp, obtained using the two different ramping rates. Equal masses were deposited in each case. These anion intensity profiles are integrated to give the instrumental response (*R*). The intensity profile as a function of the VP temperature is also plotted in each case for direct comparison (Fig. 9(c)), where it is observed that the intensity profile broadens at the higher ramping rate, which is likely a result of slow vaporization kinetics relative to the temperature increase rate.

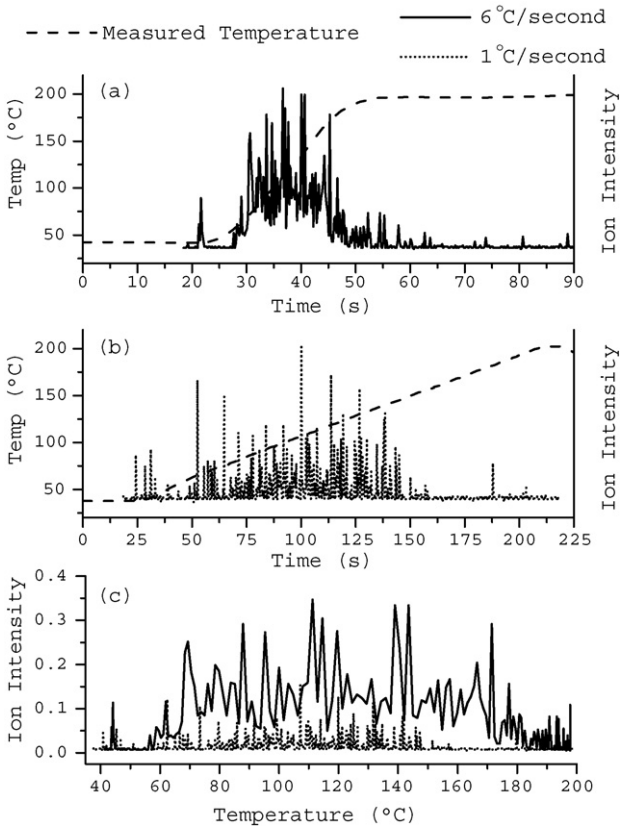

Fig. 9. Ion signal profiles for deposited oleic acid particles over time at two thermal ramping rates: (a) 6 °C/s and (b) 1 °C/s. Ion profiles for both ramping rates with source temperature is shown in (c). Total mass deposited is identical in both cases (1.8 μg). Note that the *x*-axis in (a) and (b) are in terms of time while that in (c) has been converted to temperature. Laser wavelength = 270 nm.

It is also observed, however, that a faster ramping rate improves *R*. To investigate this effect further, variable masses of pure oleic acid particles were deposited on the vaporization source and subsequently vaporized using two different ramping rates; 1 and 6 °C/s. For each ramping rate, *R* is plotted against particle mass deposited (Fig. 10). The linearity of these plots suggests that evaporative losses from the probe are not significant for collection times under 5 min, as the extent of evaporation is expected to be time-dependent. The higher sensitivity measured at the faster vaporization ramping rate is likely due to an improvement of duty cycle between the developing vapor plume and the pulsed ionization source. For faster rates of vaporization, it is expected that a higher fraction of analyte is in the vapor phase while the laser is on and the photoelectrons are present.

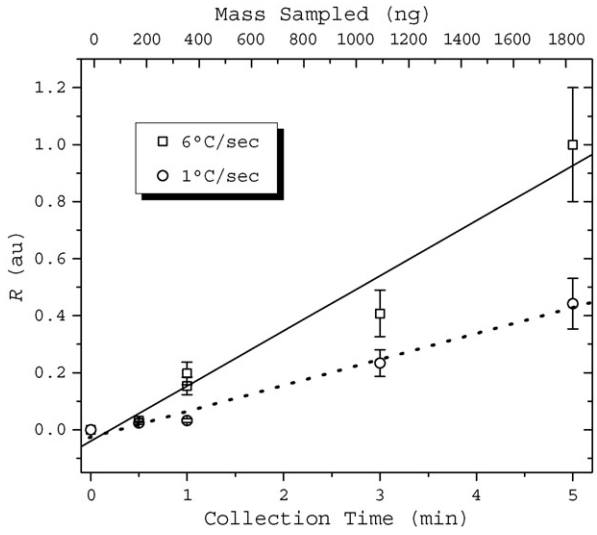

Fig. 10. Ion intensity from deposited oleic acid particles as a function of particle collection time and total mass sampled. Results are shown for signals obtained at two different thermal vaporization temperature ramping rates. Laser wavelength = 270 nm.

3.3.4. Particle phase limits of detection

The detection limit for oleic acid was determined using a differential mobility analyzer to sample monodisperse aerosol in the range 50–380 nm into the PERCI-AMS. The sample aerosol flow was monitored simultaneously using a condensation particle counter to determine the total mass sampled by the AMS. Monodisperse sampling is advantageous to eliminate variations in transmission or collection efficiency at different particle diameters. An improved vaporization source was used here, which could be ramped at a rate of 25 °C/s. Fig. 11 shows R as a function of particle diameter along with the amount of mass sampled at each diameter. Below diameters of 300 nm, R traces the mass distribution of the aerosol nicely; however, there appears to be a drop-off in sampling efficiency above 300 nm. Particle bounce-off, for example, which was found to be more common with larger particles [72], may be the source of the sampling losses [29,40,73,74]. The average detection limit across this diameter measurement range was calculated to be 30 ng. This value is approximately 5 times better than that measured for a polydisperse aerosol sample under the same temperature ramping conditions, suggesting that there may be some sampling losses at higher particle diameters, where particles carry a larger fraction of the total mass.

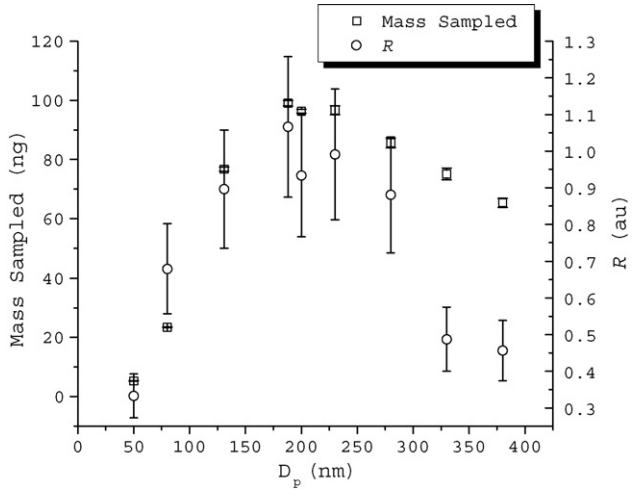

Fig. 11. Ion signals obtained from depositing monodisperse oleic acid particles ranging in diameter (D_p) from 50 to 380 nm. The total mass sampled and instrument response (R) at the corresponding diameter are both plotted. The detection limits for oleic acid calculated from this data is about 30 ng total mass sampled. Laser wavelength = 270 nm.

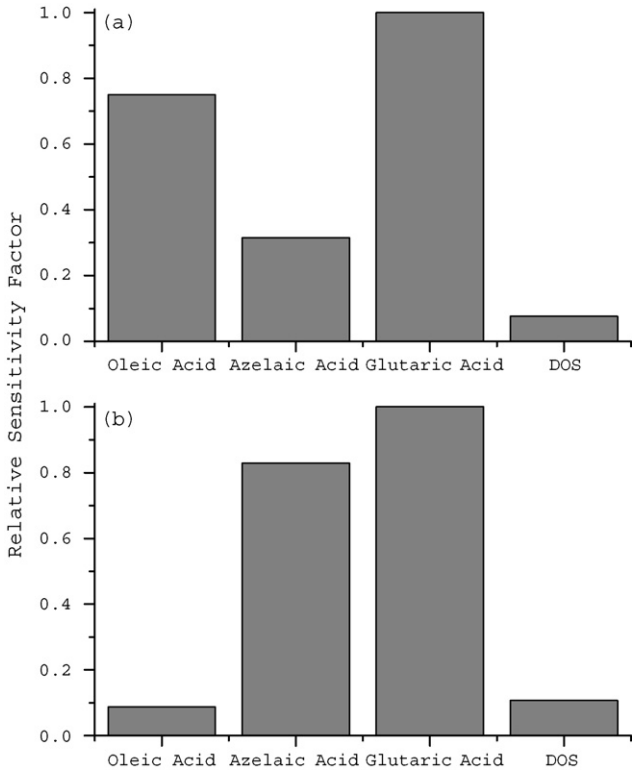

Fig. 12. Relative sensitivity factor (see definition in Section 3.3.4) for various compounds when sampled as pure aerosol (a) and internally mixed composition aerosol (b). All compounds except for dioctyl sebacate (DOS) detected as $[M-H]^-$ ion. DOS detected as $[M\text{-}243]^-$ fragment. Laser wavelength = 270 nm.

The relative sensitivities of four different particle phase compounds (oleic acid, azelaic acid, glutaric acid, and dioctyl sebacate) are compared in Fig. 12(a). Each compound was introduced as a pure, polydisperse aerosol. The sensitivity factors are calculated from the measured anion signal to background values (R/σ_{bg}) for each compound divided by the number of moles deposited and normalized to give glutaric acid a sensitivity of 1. The compounds are ordered by sensitivity as follows: DOS ≪ azelaic acid < oleic acid < glutaric acid. Limits of detection are calculated to be 2.1×10^{-8}, 5.1×10^{-9}, 2.1×10^{-9}, and 1.6×10^{-9} mol for DOS, azelaic acid, oleic acid, and glutaric acid, respectively, realizing that overestimation may occur due to size-dependent sampling losses discussed above. The differences in sensitivity reflect a combination of the physical properties of the aerosol as well as the electron capture properties of the molecules. Specifically, these properties are: transmis-

sion efficiency of the pure particles, deposition probability of the particles (including bounce-off effects and evaporation) and ionization cross section of the compound. Previous studies have shown that glutaric acid, oleic acid, and DOS form spherical particles and have high transmission efficiencies in a similar particle inlet [74]. Since DOS has the lowest vapor pressure of the group and is known to form spherical particles, its poor sensitivity is presumably a result of poor electron capture efficiency. Azelaic acid, on the other hand, forms needle-shaped particles [75], limiting the transmission efficiency through the particle inlet and increasing the probability of bounce-off [74]. Oleic acid and glutaric acid possess a favorable combination of particle shape and sensitivity to PERCI to provide low detection limits when sampled as pure aerosols.

To probe the electron capture properties of these various compounds directly, it was necessary to generate mixed particles and detect two or more compounds simultaneously. The soft ionization afforded by PERCI makes it possible to directly quantify individual compounds in mixed particles, if it is assumed that the component concentrations within the aerosol particles accurately reflect the concentrations in the aerosolized solution across all particle diameters [74]. In this manner, all compounds are sampled with identical efficiency. Fig. 12(b) shows the sensitivities calculated for each compound in a four-component mixed aerosol sample containing, oleic acid, azelaic acid, glutaric acid, and DOS (at a 1:1:1:1 molar ratio). In contrast to the pure component aerosols, azelaic acid has a significantly higher sensitivity factor, and both azelaic and glutaric acids have improved detection limits (5.1 and 4.3×10^{-10} mol, respectively). Oleic acid, conversely, has a significantly lower sensitivity factor than that for pure oleic acid particles. The decrease in sensitivity toward oleic acid has been found reproducibly when sampled as a mixed particle along with solid phase components, such as azelaic acid, stearic acid, or palmitic acid. A likely cause is a change in particle geometry of the pure vs. mixed particle, which can affect the transmission efficiency of oleic acid through the particle inlet. Transmission electron microscopy (TEM) studies have shown [76] that 50/50 (%wt) mixed oleic and stearic acid particles can have some needle-like properties that affect the aerodynamics of the particles. Further, it has been shown elsewhere [74] that sampling of mixed-phase particles through an aerodynamic focusing inlet improves transmission curves for the solid compound but inhibits, slightly, the transmission of the liquid compound.

The data in Fig. 12(b) support the hypothesis that dicarboxylic acids such as glutaric and azelaic acid will have enhanced electron capture efficiencies likely due to the presence of a second carboxylic acid group acting as an electron attachment site. By sampling an oleic/azelaic acid mixed aerosol, the relative ionization efficiencies of the two compounds can be estimated from successive measurements at variable particle collection times. R ($[M-H]^-$) for each compound is plotted (not shown) as a function of the number of moles of each compound deposited. By ratioing the slopes of these sensitivity curves, a relative ionization efficiency of 8:1 is obtained, favoring azelaic acid. This value reflects the relative electron capture cross sections for the two compounds; however, since the enhancement for azelaic acid is somewhat greater than a factor of 2, a prediction of ionization efficiency based solely on the number of carboxylic acid moieties in the molecule is an overly simplistic view. The detection limits calculated for each compound based on this experiment were 739 ng for oleic acid and 61 ng for azelaic acid. From this experiment, it is now possible to calculate the relative sampling efficiencies of the pure particles for each compound. Assuming that azelaic acid molecules are 8 times as likely to be ionized and to reach the detector as oleic acid, pure oleic acid particles are ~20 times more likely to pass through the particle inlet and deposit onto the collection/vaporization probe than pure azelaic particles.

3.3.5. *Effect of analyte vapor pressure*

The experiments described in Section 3.3.4 also demonstrate the merits of PERCI-AMS in the identification of specific compounds that may exist in complex particle mixtures. Though the aerosols discussed in this report are relatively simple mixtures, the benefits of PERCI-AMS in the analysis of chemically complex particle media have been reported previously [59]. Further, control of the vaporization process prior to PERCI analysis can provide additional selectivity for compound identification as it allows for the correlation of certain ions with the vapor pressures of their parent compounds. Even though minimal fragmentation generally occurs with PERCI, certain cases arise where fragmentation may hinder molecular identification. For example, triolein, a triglyceride commonly found in olive oil and containing three oleic acid chains, fragments to give predominately the 281 *m/z* ion, which is isobaric with the free oleic acid $[M-H]^-$ ion. However, since triolein has a significantly larger ΔH_{vap} than free oleic acid (160 kJ mol^{-1} versus 82.3 kJ mol^{-1}) [77], thermal vaporization can be used to independently measure each compound in the complex mixture [34]. Fig. 13 shows the thermal PERCI profiles of the 281 *m/z* anion intensity from oleic acid and triolein sampled separately as pure particles under identical temperature ramping conditions. The

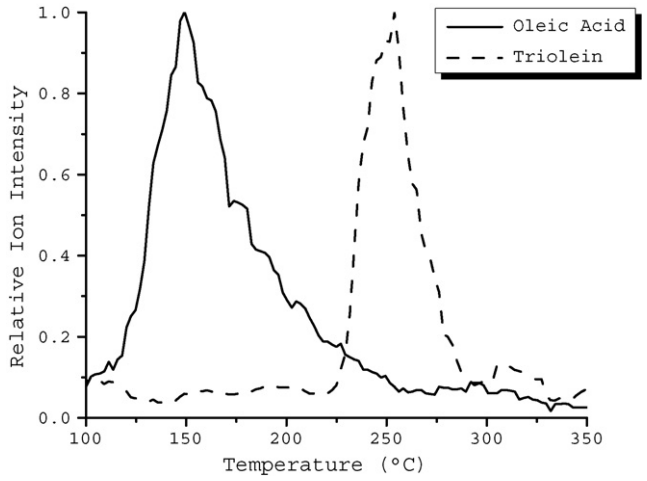

Fig. 13. Relative anion intensities for pure triolein and pure oleic acid particles deposited on the vaporization source as a function of vaporization source temperature. Both compounds detected at 281 *m/z*. Ramping rate for both profiles was 25 °C/s. Total mass sampled was 3.8 μg triolein and 3.6 μg oleic acid; laser wavelength = 270 nm.

difference in the temperature-dependence of the maximum ion signal for these two compounds illustrates the added dimension to particle analysis afforded by thermal vaporization. Note that a slower temperature ramp is ideal for resolving compounds of similar vapor pressures at the expense of sensitivity. The analysis of atmospheric particles containing unknown compound mixtures would benefit from the volatility information available from thermal vaporization [34,78].

3.4. Benefits, limitations, and future prospects of PERCI-AMS

It is relevant, here, to put the performance of the PERCI-AMS into context with other aerosol mass spectrometric methods. The primary advantage of PERCI as an ion source in aerosol mass spectrometry is the soft ionization that it affords, leading to improved capabilities for molecular identification of organic components in complex mixtures such as atmospheric aerosols as reported previously [55–59]. To further demonstrate the advantage of PERCI as a soft-ionization method, a PERCI mass spectrum is presented here (Fig. 14) of aerosolized biodiesel fuel, which is primarily composed of fatty acid methyl esters. Fatty acid methyl esters have been studied previously by PERCI-AMS [59], and it has been found that the predominant ion detected is the $[M-CH_3]^-$. The mass spectrum in Fig. 14 shows five peaks that are assigned to palmitate (255 *m/z*), linolenate (277 *m/z*), linoleate (279 *m/z*), oleate (281 *m/z*), and stearate (283 *m/z*). Additionally, the $[M-H]^-$ ion of residual glycerol, a byproduct of the *trans*-esterification reaction that produces biodiesel from a mixture of triglycerides, is detected at 91 *m/z*. Finally, some unidentified ion peaks in the range of 70–170 *m/z* appear at odd mass values and show losses of 14 and 16 mass units, consistent with a series of oxygenated hydrocarbons with varying degrees of unsaturation. A similar series of ions is found in the PERCI mass spectrum of ozonolysis products of mixed fatty acid and ester particles [59]. It is important to note that

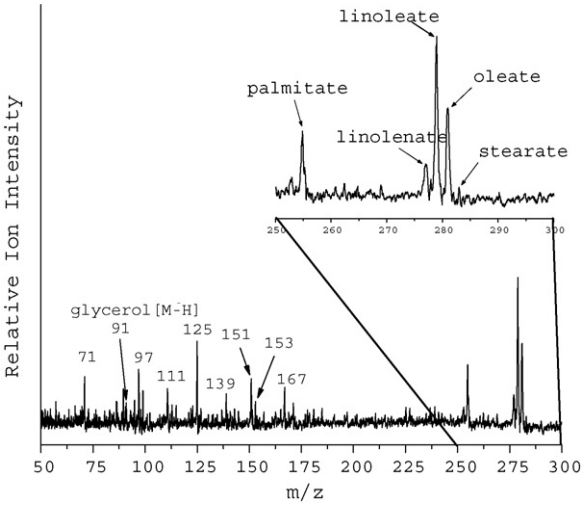

Fig. 14. PERCI mass spectrum of aerosolized biodiesel fuel showing the $[M-CH_3]^-$ ion of five fatty acid esters contained in the fuel, the $[M-H]^-$ ion of residual glycerol, and various unidentified oxygenated organic compounds.

thermal decomposition of the particle phase compounds cannot be discounted as a fragmentation channel in the PERCI-AMS; it is unclear at present what, if any, effect the thermal vaporization source has on the ionization and resulting mass spectra. Although PERCI clearly is advantageous to electron impact ionization or multi-photon ionization in terms of molecular identification, the fragmentation of the ester bond during ionization prohibits the speciation of acids versus esters without an additional level of analysis (i.e., vapor pressure, prior separation, etc.). VUV and CI have been found to be advantageous in this case, however, where esters have been detected primarily as the molecular ion [79] and $[M+H]^+$ ion [80], respectively.

In addition to the soft nature of PERCI, a benefit is the pulsed nature of PERCI which provides a high flux of photoelectrons that couples well with TOF mass analysis, providing the potential to analyze the entire organic fraction of single particles. Further, this soft-ionization method does not require a buffer gas at relatively high pressures that are necessary with the various types of positive and negative chemical ionization. This not only improves the portability of the instrument, but also permits use of PERCI with all existing mass analyses. In this regard, the most comparable aerosol mass spectrometer to the PERCI-AMS is the VUV single photon ionization, also a pulsed soft-ionization method [40,41].

The main disadvantage of the PERCI-AMS as currently configured is the low sensitivity that may limit its utility in making reliable measurements of ambient aerosol. In this respect, instruments that are based on electron impact or laser desorption ionization [26–31] are advantageous. It must be emphasized, however, that these instruments detect classes of compounds rather than individual compounds, so sensitivity is artificially improved, in a sense, since many molecules are combined into relatively few ion channels. For this reason, a comparison of detection limits for these instruments with the PERCI-AMS is not relevant. However, it should be noted that limits of detection as low as 30 pg for oleic acid have been measured with VUV SPI using IR laser vaporization [40], which is a factor of 10^3 lower than that of the PERCI-AMS.

Despite the improvements in sensitivity necessary for analysis of ambient organic aerosol by PERCI-AMS, this method, the authors believe, is attractive and worth pursuing for the potential to combine the molecular identification abilities already realized [55–59] with its potential to be a very sensitive method of aerosol analysis. To put the performance of PERCI-AMS in the context of relevant concentrations of atmospheric organic particles, a 1 min collection time would be required to sample 10 pg of oleic acid from a typical ambient atmosphere [81] (sampling at 0.45 L/min), well below the measured detection limit of 30 ng reported above. Realistically, it will be necessary, therefore, to improve the sensitivity by a factor of 10^3–10^4 if reliable atmospheric measurements are to be made at relatively non-polluted sites with reasonable particle collection times. The following discussion presents possible points in the system where significant improvements may be made in analytical performance of PERCI-AMS.

Based on gas phase detection limits given in Section 3.3.1, which range from 10^7 to 10^9 cm^{-3}, the ultimate limits of detec-

tion for aerosol samples by PERCI are expected to be well below those measured. If 10 pg of deposited oleic acid is expanded into a space of 1 cm^3, the molecular density would be 2×10^{10} cm^{-3}. Since the vaporization source is within 1 cm of the PE, the actual molecular density of oleic acid in the ionization region should be at least as high as 10^{10} cm^{-3} assuming an instantaneous and uniform expansion upon vaporization. However, as shown in the temporal profiles of the oleic acid vaporization (cf. Fig. 9(a)), the deposited oleic acid is not vaporized instantaneously, but rather over the course of about 20 s. At higher ramping rates, this can be lowered to a few seconds. Because the photoelectron burst follows closely the laser pulse, firing at 10 Hz with a pulse width of 5 ns, the method has an effective ionization duty cycle of only 5×10^{-8} (i.e., the laser is off for a vast majority of the time that the oleic acid vapor cloud is present in the ionization region). To demonstrate, a Gaussian distribution was fit to a typical oleic acid signal profile over time (not shown) at a ramping rate of 25 °C/s which was obtained from about 315 ng of deposited material. The Gaussian fit has a full width at 10% of the maximum of 2.8 s, but the laser, which fires 28 times while the vapor is present, is only on for 140 ns, or 5×10^{-8} of that time. This translates to a maximum of 15 fg of material vaporized during any one laser pulse, which, expanded into a volume of 1 cm^3, gives a pressure of 3.2×10^7 cm^{-3}. An increase in sensitivity is observed, in fact, with even the small duty cycle improvement obtained when the ramping rate is increased from 1 to 6 °C/s as discussed above. This is expected to be the primary limitation of the instrument as presently configured.

Flash vaporization of particles, as described in Section 3.3.2, provides some insight into improvements in detection capabilities with an optimized measurement duty cycle. By keeping the vaporization source at a constant temperature high enough to completely vaporize any impacting particles, the amount of analyte in the gas phase can be estimated based on the sampled particle concentration, the sampling rate, and the diffusion time of the vapor plume from individual particles. A signal to background ratio of 19 was calculated from the oleic acid signal in Fig. 7 (discussed in Section 3.3.2), which was obtained by sampling a particle concentration of 1.8×10^4 $\mu g/m^3$. The minimum particle concentration that must be sampled to produce a detectable signal is calculated to be 290 $\mu g/m^3$. While this concentration is greater than ambient levels of oleic acid, the actual particle mass that is sampled during each laser pulse is quite low. Upper and lower limits of the mass of analyte sampled may be estimated based on the laser repetition rate (10 Hz) and the laser pulse duration (5 ns), respectively. At the upper limit, assuming molecules present at the PE surface are ionized and extracted away from the ionization region with 100% efficiency with each laser pulse and subsequent extraction pulse, the total aerosol mass sampled is equal to the amount sampled between laser pulses or 100 ms; at the lower limit, the smallest aerosol mass that can be sampled is the amount that enters the system during the 5 ns laser pulse, which assumes that the particle vapors diffuse through the ionization region and are pumped away in under 5 ns. A better estimate, however, can be calculated [82], assuming a Maxwell-Boltzmann distribution of the vaporized molecules over time, based on VP temperature, molecular weight, and distance to the ionization region. Using this relationship to predict the behavior of oleic acid in our system (assuming a similar ionization region volume to that used in reference [82]), the vapor plume from a single oleic acid particle is expected to lead to a temporal distribution of analyte within the ionization region with a full width at 10% of the maximum of 45 μs.

Table 1
Three estimates (upper, lower, and best) of the residence time for the vapor plume of single particles in the ionization region and the resulting estimated mass present during any given laser pulse

Estimated residence time in ionization region	Mass concentration sampled ($\mu g/m^3$)	Total mass in ionization region (g)	# of particles vaporized
100 ms	290	2.2×10^{-10}	30000
45 μs	290	9.8×10^{-14}	13.5
5 ns	290	1.1×10^{-17}	1.5×10^{-3}

The mass concentration sampled is the calculated LOD using flash vaporization mode. The number of particles vaporized during the residence time is calculated in each case assuming an average particle diameter of 250 nm.

Table 1 shows estimates for the mass of oleic acid vapor in the ionization region necessary to provide a detectable signal in each of the three cases. The number of particles sampled is calculated assuming a particle diameter of 250 nm, which is a typical mean particle diameter in our experiments. With higher estimated residence times, the number of vaporized particles that contribute to the oleic acid vapor phase in the ionization region increases. Even at the highest possible residence time, which is quite unrealistic, the sampled mass necessary for detection is about 220 pg. This mass can be sampled from a typical ambient atmosphere in 20 min. Using the 45 μs as a reasonable estimate for build up of vapor in the ionization region, the necessary sampled mass is on the order of 100 fg, which can be sampled from an ambient atmosphere in 600 ms. This thought experiment yields the best possible detection limits for the PERCI-AMS without any improvement in delivery of particles from the atmosphere, through the particle inlet, to the vaporization source and without any improvement of the TOF-MS efficiency or detection electronics. The difference between these values and that reported above for the detection limit of deposited oleic acid (30 ng), represents the potential for improvement to the PERCI-MS with respect to losses after the particles impact the vaporization source, including "bounce-off," evaporative losses, and, most significantly, losses from a low duty cycle of the ionization.

A significant improvement in duty cycle could be obtained by either (a) increasing the pulse rate of the PERCI photon source; (b) synchronizing the ionization pulse with the arrival of single particles at a continuously heated VP or (c) adapting to a pulsed vaporization source. Option (a) is probably the least feasible because the pulse rate is limited by the practical considerations of data collection speed and the fact that most commercially available UV lasers cannot pulse above 10^1 Hz. Option (b) could be achieved using laser velocimetry [35,82,83] to measure the time-of-flight of sampled particles, thereby predicting the arrival of each particle at the vaporization source. The laser pulse can then be synchronized to overlap in time

with the resulting vapor plume. Based on the estimates given above, laser velocimetry could be employed in our system to allow for detection of single particles containing at least 100 fg of oleic acid. This corresponds to a pure oleic acid particle of about 600 nm. Option (c) would be most successfully achieved using IR laser vaporization. IR vaporization has been adapted successfully to aerosol mass spectrometers with laser ionization sources using both CO_2 [84–86] and Nd:YAG lasers [40]. The large size of CO_2 lasers is prohibitive for field applications, however, YAG lasers are small enough to be practical. IR laser vaporization allows for a synchronous vaporization and ionization scheme, vastly improving the duty cycle. A study by Oktem et al. [40], for example, suggested that an improvement of approximately 3–4 orders of magnitude was obtained in going from thermal vaporization to IR laser vaporization when coupled to a pulsed VUV photoionization source: a result in line with our estimates. Additional means for improving the sensitivity of the PERCI-AMS include: pre-concentration of the sampled aerosol, for example, using the VACES system [87,88] as demonstrated with two different aerosol mass spectrometers by Khlystov et al. [89] and Zhao et al. [90], and cryogenic cooling of the vaporization probe to decrease evaporative losses of the deposited particles.

4. Conclusions

PERCI has been shown here and elsewhere [55–59] to be a soft and sensitive ionization method, suited for the analysis of particle- and gas-phase organics. The experiments performed here have provided a detailed characterization of the processes that contribute to the ionization and detection of particle-bound organic compounds by PERCI-AMS including: particle transmission, photoelectron generation and emission, particle vaporization, molecule–electron interaction, and anion energetics and fate. The factors that have been found to affect the performance of the PERCI-AMS include: delayed pulse extraction time, relative positioning of the vaporization probe and photoelectrode, laser intensity, analyte pressure in the ionization region, particle matrix, and vaporization source ramping rate. It has been shown that PERCI leads to the generation of high instantaneous currents (∼100 mA) of low energy photoelectrons available for attachment to neighboring molecules with minimal fragmentation. Analysis of complex mixtures, therefore, is greatly aided by the capabilities of PERCI to identify and quantify individual organic components. Further, the combination of thermal vaporization with PERCI provides an additional level of selectivity as vapor pressure dependent mass spectra can further aid molecular identification. Gas phase detection limits have been shown to be on the orders of 10^7–10^9 cm^{-3} and particle phase detection limits for individual compounds are found to be on the orders of 10^{-8}–10^{-7} g of total deposited mass. Matrix-dependent sampling efficiencies (based on differences in particle size and geometry), observed here and by others [29,40,59,73,74], present a significant barrier to extending analyte sensitivity measurements performed with lab-generated aerosols to quantification of specific compounds in ambient atmospheric aerosol.

With this thorough characterization of the PERCI-AMS completed, the limitations of the instrument as presently constructed are well understood. Relatively simple and inexpensive improvements can be made, including modifications to the vaporization source to allow for faster temperature ramping and optimization of the geometry of the vaporization source to minimize particle bounce-off. The most significant area for improvement, however, will likely involve the adaptation of IR laser vaporization of deposited particles. The duty cycle improvement expected from a synchronized vaporization and ionization event is likely to improve the detection limits by approximately 3–4 orders of magnitude, which would allow for measurements of oleic acid, as well as other relevant organic compounds, at levels expected under ambient conditions.

Acknowledgements

The authors gratefully acknowledge the financial support of the National Science Foundation (ATM-0440074), the American Society for Mass Spectrometry, VT-EPSCoR, and the National Center for Environmental Research (NCER) STAR Program, EPA (Fellowship 91615301-0). The authors would also like to thank Scott Gordon for providing the sample of biodiesel.

References

[1] A.L. Hunt, G.A. Petrucci, TRAC-Trends Anal. Chem. 21 (2002) 74.
[2] R.C. Sullivan, K.A. Prather, Anal. Chem. 77 (2005) 3861.
[3] T.M. Raymond, S.N. Pandis, J. Geophys. Res. 107 (2002) 4787.
[4] N.C. Shantz, W.R. Leaitch, P.F. Caffrey, J. Geophys. Res. 108 (2003) 4168.
[5] M. Mircea, M.C. Facchini, S. Decesari, F. Cavalli, L. Emblico, S. Fuzzi, A. Vestin, J. Rissler, E. Swietlicki, G. Frank, M.O. Andreae, W. Maenhaut, Y. Rudich, P. Artaxo, Atmos. Chem. Phys. 5 (2005) 3111.
[6] K.E.H. Hartz, T. Rosenorn, S.R. Ferchak, T.M. Raymond, M. Bilde, N.M. Donahue, S.N. Pandis, J. Geophys. Res. 110 (2005) D14208.
[7] U. Lohmann, C. Leck, Tellus Ser. B-Chem. Phys. Meteorol. 57 (2005) 261.
[8] T.M. VanReken, N.L. Ng, R.C. Flagan, J.H. Seinfeld, J. Geophys. Res. 110 (2005) D07206.
[9] M. Bilde, B. Svenningsson, Tellus Ser. B-Chem. Phys. Meteorol. 56 (2004) 128.
[10] M. Mircea, M.C. Facchini, S. Decesari, S. Fuzzi, R.J. Charlson, Tellus Ser. B-Chem. Phys. Meteorol. 54 (2002) 74.
[11] E. Andrews, S.M. Kreidenweis, J.E. Penner, S.M. Larson, J. Geophys. Res. 102 (1997) 21997.
[12] C.N. Cruz, S.N. Pandis, Atmos. Environ. 31 (1997) 2205.
[13] M. Kanakidou, J.H. Seinfeld, S.N. Pandis, I. Barnes, F.J. Dentener, M.C. Facchini, R. Van Dingenen, B. Ervens, A. Nenes, C.J. Nielsen, E. Swietlicki, J.P. Putaud, Y. Balkanski, S. Fuzzi, J. Horth, G.K. Moortgat, R. Winterhalter, C.E.L. Myhre, K. Tsigaridis, E. Vignati, E.G. Stephanou, J. Wilson, Atmos. Chem. Phys. 5 (2005) 1053.
[14] G.B. Ellison, A.F. Tuck, V. Vaida, J. Geophys. Res. 104 (1999) 11633.
[15] M.S. Jang, N.M. Czoschke, S. Lee, R.M. Kamens, Science 298 (2002) 814.
[16] T. Moise, Y. Rudich, J. Phys. Chem. A 106 (2002) 6469.
[17] R. Broske, J. Kleffmann, P. Wiesen, Atmos. Chem. Phys. 3 (2003) 469.
[18] T.S. Hiura, N. Li, R. Kaplan, M. Horwitz, J.C. Seagrave, A.E. Nel, J. Immunol. 165 (2000) 2703.
[19] N. Li, M.I. Venkatesan, A. Miguel, R. Kaplan, C. Gujuluva, J. Alam, A. Nel, J. Immunol. 165 (2000) 3393.
[20] A.M. Casillas, T. Hiura, N. Li, A.E. Nel, Ann. Allergy, Asthma Immunol. 83 (1999) 624.
[21] H. Takenaka, K. Zhang, D. Diazsanchez, A. Tsien, A. Saxon, J. Allergy Clin. Immunol. 95 (1995) 103.

[22] N. Li, M.Y. Wang, T.D. Oberley, J.M. Sempf, A.E. Nel, J. Immunol. 169 (2002) 4531.
[23] T.S. Hiura, M.P. Kaszubowski, N. Li, A.E. Nel, J. Immunol. 163 (1999) 5582.
[24] Y. Kumagai, S. Koide, K. Taguchi, A. Endo, Y. Nakai, T. Yoshikawa, N. Shimojo, Chem. Res. Toxicol. 15 (2002) 483.
[25] P.H. McMurry, Atmos. Environ. 34 (2000) 1959.
[26] C.A. Noble, K.A. Prather, Environ. Sci. Technol. 30 (1996) 2667.
[27] P.G. Carson, K.R. Neubauer, M.V. Johnston, A.S. Wexler, J. Aerosol Sci. 26 (1995) 535.
[28] P.J. McKeown, M.V. Johnston, D.M. Murphy, Anal. Chem. 63 (1991) 2069.
[29] J.T. Jayne, D.C. Leard, X.F. Zhang, P. Davidovits, K.A. Smith, C.E. Kolb, D.R. Worsnop, Aerosol Sci. Technol. 33 (2000) 49.
[30] K.P. Hinz, R. Kaufmann, B. Spengler, Aerosol Sci. Technol. 24 (1996) 233.
[31] D.M. Murphy, D.S. Thomson, Aerosol Sci. Technol. 22 (1995) 237.
[32] P.J. Silva, K.A. Prather, Anal. Chem. 72 (2000) 3553.
[33] Q. Zhang, M.R. Alfarra, D.R. Worsnop, J.D. Allan, H. Coe, M.R. Canagaratna, J.L. Jimenez, Environ. Sci. Technol. 39 (2005) 4938.
[34] H.J. Tobias, P.J. Ziemann, Anal. Chem. 71 (1999) 3428.
[35] P.T.A. Reilly, R.A. Gieray, M. Yang, W.B. Whitten, J.M. Ramsey, Anal. Chem. 69 (1997) 36.
[36] J.D. Hearn, G.D. Smith, Anal. Chem. 76 (2004) 2820.
[37] D. Voisin, J.N. Smith, H. Sakurai, P.H. McMurry, F.L. Eisele, Aerosol Sci. Technol. 37 (2003) 471.
[38] T. Hoffmann, R. Bandur, S. Hoffmann, B. Warscheid, Spectroc. Acta Pt. B-At. Spectrosc. 57 (2002) 1635.
[39] A.C. Lazar, P.T.A. Reilly, W.B. Whitten, J.M. Ramsey, Anal. Chem. 72 (2000) 2142.
[40] B. Oktem, M.P. Tolocka, M.V. Johnston, Anal. Chem. 76 (2004) 253.
[41] E. Woods III, G.D. Smith, Y. Dessiaterik, T. Baer, R.E. Miller, Anal. Chem. 73 (2001) 2317.
[42] A. Chutjian, A. Garscadden, J.M. Wadehra, Phys. Rep. 264 (1996) 393.
[43] H. Adboul-Carime, M.A. Huels, F. Brüning, E. Illenberger, L. Sanche, J. Chem. Phys. 113 (2000) 2517.
[44] M.T. Bernius, A. Chutjian, Anal. Chem. 62 (1990) 1345.
[45] A. Modelli, J. Phys. Chem. A 109 (2005) 6193.
[46] S. Boumsellek, S.H. Alajajian, A. Chutjian, J. Am. Soc. Mass Spectrom. 3 (1992) 243.
[47] A. Modelli, M. Venuti, Int. J. Mass Spectrom. 205 (2001) 7.
[48] E. Camera, D. Pravisani, Anal. Chem. 39 (1967) 1645.
[49] U.B. Imashev, O.G. Khvostenko, V.G. Lukin, V.G. Shereshovets, V.A. Mazunov, J. Anal. Chem. 53 (1998) 578.
[50] U.B. Imashev, O.G. Khvostenko, V.G. Lukin, R.R. Vezirov, I.R. Khairudinov, R.F. Tuktarov, V.A. Mazunov, J. Anal. Chem. 53 (1998) 779.
[51] S. Tobita, M. Meinke, E. Illenberger, L.G. Christophorou, H. Baumgartel, S. Leach, Chem. Phys. 161 (1992) 501.
[52] J.H. Wei, S.Y. Liu, S.A. Fedoreyev, V.G. Voinov, Rapid Commun. Mass Spectrom. 14 (2000) 1689.
[53] V.G. Voinov, V.M. Boguslavskiy, Y.N. Elkin, Org. Mass Spectrom. 29 (1994) 641.
[54] J.A. Laramée, P. Mazurkiewicz, V. Berkout, M.L. Deinzer, Mass Spectrom. Rev. 15 (1996) 15.
[55] B.W. LaFranchi, G.A. Petrucci, J. Am. Soc. Mass Spectrom. 15 (2004) 424.
[56] B.W. LaFranchi, J. Zahardis, G.A. Petrucci, Rapid Commun. Mass Spectrom. 18 (2004) 2517.
[57] J. Zahardis, B.W. LaFranchi, G.A. Petrucci, J. Geophys. Res. 110 (2005) D08307.
[58] J. Zahardis, B.W. LaFranchi, G.A. Petrucci, Atmos. Environ. 40 (2006) 1661.
[59] J. Zahardis, B.W. LaFranchi, G.A. Petrucci, Int. J. Mass Spectrom. 253 (2006) 38.
[60] J. Zahardis, B.W. LaFranchi, G.A. Petrucci, Eur. J. Lipid Sci. Technol., submitted for publication.
[61] P. Liu, P.J. Ziemann, D.B. Kittelson, P.H. McMurry, Aerosol Sci. Technol. 22 (1995) 314.
[62] P. Liu, P.J. Ziemann, D.B. Kittelson, P.H. McMurry, Aerosol Sci. Technol. 22 (1995) 293.
[63] G.A. Petrucci, P.B. Farnsworth, P. Cavalli, N. Omenetto, Aerosol Sci. Technol. 33 (2000) 105.
[64] Y. Kawamura, K. Toyoda, M. Kawai, J. Appl. Phys. 71 (1992) 2507.
[65] T.L. Gilton, J.P. Cowin, G.D. Kubiak, A.V. Hamza, J. Appl. Phys. 68 (1990) 4802.
[66] A. Hadjiantoniou, L.G. Christophorou, J.G. Carter, J. Chem. Soc. Faraday Trans. II 69 (1973) 1691.
[67] L.G. Christophorou, A. Hadjiantoniou, J.G. Carter, J. Chem. Soc. Faraday Trans. II 69 (1973) 1713.
[68] J.P. Johnson, D.L. McCorkle, L.G. Christophorou, J.G. Carter, J. Chem. Soc. Faraday Trans. II 71 (1975) 1742.
[69] B. Spengler, R.J. Cotter, Anal. Chem. 62 (1990) 793.
[70] G.Z. Li, H.S. Kim, S.H. Guan, A.G. Marshall, J. Am. Chem. Soc. 119 (1997) 2267.
[71] R.A. Duce, V.A. Mohnen, P.R. Zimmerman, D. Grosjean, W. Cautreels, R. Chatfield, R. Jaenicke, J.A. Ogren, E.D. Pellizzari, G.T. Wallace, Rev. Geophys. 21 (1983) 921.
[72] W.C. Hinds, Aerosol Technology, John Wiley & Sons, New York, NY, 1982.
[73] M.P. Sinha, C.E. Giffin, D.D. Norris, T.J. Estes, V.L. Vilker, S.K. Friedlander, J. Colloid Interface Sci. 87 (1982) 140.
[74] H.J. Tobias, P.M. Kooiman, K.S. Docherty, P.J. Ziemann, Aerosol Sci. Technol. 33 (2000) 170.
[75] The Merck Index: An Encyclopedia of Chemicals, Drugs, and Biologicals, 12th, Merck & Co., Whitehouse Station, NJ, 1996.
[76] Y. Katrib, G. Biskos, P.R. Buseck, P. Davidovits, J.T. Jayne, M. Mochida, M.E. Wise, D.R. Worsnop, S.T. Martin, J. Phys. Chem. A 109 (2005) 10910.
[77] J.S. Chickos, W.E. Acree, J. Phys. Chem. Ref. Data 32 (2003) 519.
[78] S. Chattopadhyay, D.J. Tobias, P. Ziemann, Anal. Chem. 73 (2001) 3797.
[79] M.P. Tolocka, K.J. Heaton, M.A. Dreyfus, S.Y. Wang, C.A. Zordan, T.D. Saul, M.V. Johnston, Environ. Sci. Technol. 40 (2006) 1843.
[80] J.D. Hearn, A.J. Lovett, G.D. Smith, Phys. Chem. Chem. Phys. 7 (2005) 501.
[81] W.F. Rogge, M.A. Mazurek, L.M. Hildemann, G.R. Cass, B.R.T. Simoneit, Atmos. Environ. Part A 27 (1993) 1309.
[82] D.C. Sykes, E. Woods III, G.D. Smith, T. Baer, R.E. Miller, Anal. Chem. 74 (2002) 2048.
[83] E. Gard, J.E. Mayer, B.D. Morrical, T. Dienes, D.P. Fergenson, K.A. Prather, Anal. Chem. 69 (1997) 4083.
[84] E. Woods III, G.D. Smith, R.E. Miller, T. Baer, Anal. Chem. 74 (2002) 1642.
[85] E. Woods III, R.E. Miller, T. Baer, J. Phys. Chem. A 107 (2003) 2119.
[86] A. Zelenyuk, J. Cabalo, T. Baer, R.E. Miller, Anal. Chem. 71 (1999) 1802.
[87] S. Kim, P.A. Jaques, M.C. Chang, J.R. Froines, C. Sioutas, J. Aerosol Sci. 32 (2001) 1281.
[88] S. Kim, P.A. Jaques, M.C. Chang, T. Barone, C. Xiong, S.K. Friedlander, C. Sioutas, J. Aerosol Sci. 32 (2001) 1299.
[89] A. Khlystov, Q. Zhang, J.L. Jimenez, C. Stanier, S.N. Pandis, M.R. Canagaratna, P. Fine, C. Misra, C. Sioutas, J. Aerosol Sci. 36 (2005) 866.
[90] Y. Zhao, K.J. Bein, A.S. Wexler, C. Misra, P.M. Fine, C. Sioutas, J. Geophys. Res. 110 (2005).